SNAIL is Induced by Tamoxifen and Leads to Growth Inhibition in Invasive Lobular Breast Carcinoma

Emily A. Bossart[1,2,‡], **Nilgun Tasdemir**[1,2,‡], **Matthew J. Sikora**[3], **Amir Bahreini**[2,4], **Kevin M. Levine**[2,5], **Jian Chen**[2], **Ahmed Basudan**[2,6], **Britta M. Jacobsen**[3], **Timothy F. Burns**[1,7], and **Steffi Oesterreich**[1,2,*]

[1]Department of Pharmacology & Chemical Biology, University of Pittsburgh School of Medicine, Pittsburgh, PA 15261, USA

[2]Women's Cancer Research Center, Magee-Womens Research Institute, University of Pittsburgh Cancer Institute, 204 Craft Avenue, Pittsburgh, PA 15213, USA

[3]Department of Pathology, University of Colorado Anschutz Medical Campus, Denver, CO 80045, USA

[4]Department of Genetics and Molecular Biology, School of Medicine, Isfahan University of Medical Sciences, Isfahan Province, Isfahan, Iran

[5]Department of Pathology, University of Pittsburgh School of Medicine, PA 15261, USA

[6]Department of Human Genetics, University of Pittsburgh School of Public Health, Pittsburgh, PA 15261, USA

[7]Department of Medicine, UPMC Hillman Cancer Center, Pittsburgh, PA 15232, USA

Abstract

PURPOSE: Invasive lobular carcinoma (ILC) is a histological subtype of breast cancer that is predominantly estrogen receptor alpha (ER)-positive (+), and is thus treated with endocrine therapies. Herein, we sought to understand the molecular underpinnings of the 4-hydroxytamoxifen (4OHT) resistance in ILC by assessing the potential role of the epithelial-to-mesenchymal transition transcription factor (EMT-TF) SNAIL (*SNAI1*).

METHODS: Using a series of breast cancer cell lines, we measured the basal, estrogen and 4OHT-induced expression of SNAIL and other EMT-TF family members by quantitative reverse transcription- polymerase chain reaction and immunoblotting. Chromatin immunoprecipitation experiments were performed to assess ER binding to the SNAIL promoter. Cell proliferation, cell cycle and apoptosis were assessed in 2D cultures. 3D growth was assessed in Matrigel and Collagen I cultures.

---

*Corresponding Author (oesterreichs@upmc.edu).
‡Equal contributors

RESULTS: Estrogen and 4OHT induced SNAIL expression, but not that of the other EMT-TF family members SLUG (*SNAI2*) and SMUC (*SNAI3*), with the 4OHT effect being specific to the lobular but not the ductal subtype. We observed estrogen and 4OHT-induced ER recruitment to the *SNAI1* promoter and high endogenous basal levels of SNAIL and several EMT-TFs in ILC cell lines. While SNAIL knockdown had a minor impact on the 4OHT partial agonism in estrogen-depleted conditions, it led to a surprising increase in cell proliferation in full serum. In complementary experiments, inducible *SNAI1* overexpression caused decreased proliferation, associated with a cell cycle arrest in G_0/G_1. Additionally, apoptosis was observed in BCK4 cells.

CONCLUSION: These data suggest a previously unrecognized role for SNAIL in ILC, substantiating a context-dependent behavior for this EMT-TF.

Introduction

Breast cancer is the most prevalent malignancy for women in the United States, impacting an estimated 252,710 women in 2017 [1, 2]. The two major histological subtypes of breast cancer are Invasive Lobular Carcinoma (ILC) and Invasive Ductal Carcinoma (IDC) [3–6]. ILC is characterized by the loss of the epithelial marker E-cadherin, which leads to the characteristic growth of ILC tumor cells throughout the stroma in discohesive linear cords within dense extracellular matrix (ECM) [8, 9]. Other unique aspects of ILC include its difficulty to be detected by imaging modalities, likely due to its diffuse growth pattern, and increased metastases to the gastrointestinal tract, peritoneum and ovaries [10–13]. These histological and clinical differences underscore the importance of understanding and treating ILC as a distinct disease and highlight the need to explore the mechanisms of its unique biology.

As ILCs are predominantly estrogen receptor alpha (ER) positive (+), patients are treated with endocrine therapies such as Selective Estrogen Receptor Modulators (SERMs), Aromatase Inhibitors (AIs), and Selective Estrogen Receptor Degraders (SERDs) [14, 15]. Endocrine therapy for breast cancer has remained one of the most successful types of targeted therapy among all cancers [16]. However, recurrence remains a critical issue in breast cancer as tumor cells evade treatment and regrow at primary and metastatic sites [17, 18]. Despite exhibiting favorable prognostic and predictive factors for endocrine therapy such as high ER expression and low proliferation rates, patients with ILC experience a higher frequency of long-term recurrences, often arising many years post primary lesion diagnosis [15, 19–22]. A better understanding of the mechanistic responses of ILC tumors to endocrine therapies is critically needed to improve the outcomes of patients with ILC.

The SERM Tamoxifen exhibits mixed agonist/antagonist activities and has been well characterized for its potential to select resistant cell populations with increased tumorigenic phenotypes, often driven by increased PI3K/MAPK signaling [23–25]. More specifically in the lobular subtype, our lab recently identified *de novo* tamoxifen resistance in MDA-MB-134-VI cells [26], showing that these cells recognize SERMs including 4-

hydroxytamoxifen (4OHT, active tamoxifen metabolite) as partial agonists that can drive cell proliferation. As part of our efforts to understand the underlying mechanisms of this phenotype, our gene expression analyses identified *SNAI1* (encoding the transcription factor SNAIL) as the top 4OHT-induced gene in these cells [26]. SNAIL, and its related family members SLUG and SMUC, are transcription factors (TFs) that regulate epithelial-to-mesenchymal transition (EMT) [18, 27]. In breast cancer, high expression of EMT-TFs is associated with increased tumor grade, progression and metastasis [28–32]. Consistent with this, SNAIL expression has been shown to promote cellular resistance to programmed cell death, and to alter response to genotoxic stress [33–35].

The few studies focused on SNAIL in ILC [36, 37] so far have been limited to descriptive expression analyses in clinical samples without any functional or mechanistic interrogation. Based on the known association of *SNAI1*/SNAIL with aggressive tumor phenotypes, we hypothesized that the induction of *SNAI1* (and/or other EMT-TFs) by SERMs could mediate the endocrine resistance programs in ILC cells. Here we show that the levels of SNAIL (but not those of the closely related family members SLUG and SMUC) are regulated by 4OHT, which is associated with 4OHT-mediated recruitment of ER to the *SNAI1* promoter. This phenomenon was strongly context-dependent as it was only seen in ILC but not in IDC cell lines. While stable knockdown of SNAIL proved to be challenging, reflecting tight regulation of its expression in ILC cells, transient inhibition led to only a minor impact on 4OHT partial agonism, along with an unexpected increase in cell proliferation in full serum. Conversely, inducible SNAIL overexpression caused a decrease in 2D and 3D growth, suggesting previously unrecognized and hormone-independent roles for SNAIL in tumorigenesis that warrant further investigation in future studies.

Materials and Methods

Cell Culture and plasmids

MCF-7, T47D, MDA-MB-231, MDA-MB-134-VI and MDA-MB-330 cell lines were purchased from the American Tissue Culture Collection (ATCC), and Sum44PE cells were purchased from Asterand. BCK4 were obtained from the Jacobsen Laboratory [38]. All cell lines were tested to be mycoplasma free every six months using MycoAlert™ Mycoplasma Detection Kit (Lonza[#]LT07–418) and were authenticated by the University of Arizona Genetics Core by Short Tandem Repeat (STR) DNA profiling. Authenticated cells were kept in continuous culture for <6 months. Cells were cultured as previously described [26, 39], except for the use of 5% Fetal Bovine Serum (FBS) (Gibco[#]26140) for MCF-7, MDA-MB-231 and BCK4 cells. Cells were deprived of exogenous steroid hormones as previously described [26]. Estradiol (E2) (Sigma[#]E2758) and 4-hydroxytamoxifen (4OHT) (Sigma[#]H6278) were dissolved in Dimethylsulfoxide (DMSO) (ATCC[#]4-X-5) and used at the indicated conditions. For inducible SNAIL overexpression, an entry clone containing *SNAI1* ORF (a kind gift from Dr. Timothy Burns) was cloned into pINDUCER20 (ref [40]; Addgene Plasmid[#]44012) using Gateway™ LR Clonase™ II and standard manufacturer's protocol (Invitrogen[#]11791100). Stable cell lines were generated by lentiviral transduction as previously described [40] and maintained in 1.25 mg/mL Geneticin (Thermo Fisher

Scientific[#]10131–035). To induce overexpression, cells were treated with 0.5 μg/mL Doxycycline (Sigma[#]D9891–1G) one day after plating.

Reverse Phase Protein Array (RPPA), Immunoblotting and Chromatin Immunoprecipitation (ChIP) Assays

RPPA assays were performed as previously described [26]. Briefly, MDA-MB-134-VI and Sum44PE cells were seeded at 70–80% confluence in full serum or estrogen-deprived conditions and treated with 1 nM E2 or vehicle (Ethanol) for 24 hours. Samples were collected in MD Anderson RPPA lysis buffer and assessed at the Functional Proteomics Core of MD Anderson. For immunoblotting, proteins were extracted using either MD Anderson RPPA or RIPA buffer and assayed using the Odyssey Infrared Imaging system (LiCor). The primary antibodies used are listed in Supplementary Table 1. ChIP assays were performed in two independent experiments as previously described using IgG or ERα (Santa Cruz HC-20[#]sc-543) antibodies [26, 41]. ChIP Quantitative Reverse Transcription Polymerase Chain Reactions (qRT-PCR) were performed using input samples diluted 1:5 and samples diluted 1:3 with 5 μL/technical replicate well using the primers listed in Supplementary Table 2. Data were analyzed using fold enrichment (FE) over IgG controls. The intensities of the bands in the immunoblots were quantified using Image J. Detailed methods are included in Supplementary Text.

qRT-PCR

mRNA was isolated from triplicate samples using either manufacturer's protocol of the illustra RNAspin Mini Kit (GE Healthcare[#]25-0500-72) or NucleoSpin RNA Kit (Takara Clontech[#]740955.250). 250–500 ng of mRNA were converted into cDNA using 1X iScript (BioRad[#]1708891) manufacturer's protocol. Samples were assessed by qRT-PCR using SsoAdvanced™ Universal SYBR® Green Supermix (BioRad[#]1725274) using the primers listed in Supplementary Table 3 All qRT-PCRs were performed in two to three independent experiments with data normalized to the housekeeping gene *RPLP0.*

Transient Knockdown Assays

Cells were reverse transfected using Lipofectamine™ RNAiMAX following manufacturer's protocol (Thermo Fisher Scientific[#]13778-150) with 10 nM final concentration of ON-TARGETplus Non-Targeting Control Pool (Dharmacon[#]D-001810-10) or Human *SNAI1* Pool (Dharmacon[#]L-010847-01) siRNA in Opti-MEM® I (Gibco[#]31985-070) for 24–48 hours prior to downstream applications.

2D and 3D Growth Assays

For 2D assays, cells were plated in technical replicates of 3–6 at 15,000 (ILC; all experiments except Supplementary Fig. 5 at 5,000) or 5,000 (IDC) cells/well and proliferation was assessed as recently described [26] using FluoReporter™ Blue Fluorometric dsDNA Quantitation Kit (Invitrogen[#]F2962). Data were captured using VictorX Software on a PerkinElmer plate reader and plotted after correction to background media fluorescence. Non-linear regressions fitted to each data set were used to test

differences in rates of growth. Matrigel and Collagen I embedding assays were done as previously described [39]. Details are included in Supplementary Text.

Mammosphere Assay

Mammospheres were generated and processed as previously described [39, 42]. Briefly, cells were cultured in triplicate wells of 6-well Ultra Low Attachment Plates (Corning#3471) in mammosphere media (1:1 DMEM/Ham's F-12 media, 20 ng/mL bFGF (BD Biosciences#354060), 20 ng/mL EGF (BD Biosciences#354001), B27 (Gibco#17504), 2.5 mL Penicillin/Streptomycin, and 4 μg/mL Heparin (Sigma#H4784)). Detailed methods are included in Supplementary Text.

Cell Cycle and Apoptosis Assays

Cells were seeded at 300,000/well in 6-well plates in triplicates and incubated with dox for 4 days. Cells were harvested, washed with PBS and stained with Hoechst for cell cycle analysis or with Annexin V/PI using APC-Annexin V (BD Biosciences; #550474) for apoptosis analysis following the manufacturer's protocol. Samples were acquired on an LSR II Flow cytometer (BD Biosciences) and analyzed using BD FACSDiva software (BD Biosciences).

Results

SNAI1 Expression is Induced by E2 and 4OHT in ER+ ILC Cells

We recently reported that E2 induces the expression of a large number of genes at the RNA level in the ER+ ILC cell lines MDA-MB-134-VI and Sum44PE, including the EMT-TF *SNAI1* [26]. We first validated this finding in an extended panel of ER+ ILC (including BCK4 and MDA-MB-330) and IDC (MCF7 and T47D) cells by qRT-PCR following E2 deprivation and E2 treatment (Fig. 1a). This analysis showed significant E2-mediated induction of *SNAI1* in MDA-MB-134-VI and in MCF-7, with a trend for induction in Sum44PE, BCK4 and T47D cells, consistent with a previous report [43]. Importantly, this induction was specific to *SNAI1* and not observed for the other EMT-TFs *SNAI2* and *SNAI3* (Supplementary Fig. 1a).

To assess if E2 can induce *SNAI1* (and potentially other EMT-related genes) at the protein level, we performed Reverse Phase Protein Arrays (RPPA) on MDA-MB-134-VI and Sum44PE cell lines maintained either in full serum (FS), or switched to charcoal-stripped serum (E2-deprived [Cont]) and subsequently treated with 1 nM E2 for 24 hours (E2). This analysis revealed that E2 also induces the expression of SNAIL protein in MDA-MB-134-VI cells, with some modest induction also in Sum44PE (Fig. 1b), mirroring the induction of mRNA levels. Of note, other EMT-related proteins on the RPPA such as P-cadherin, Fibronectin, and c-kit were not significantly induced by E2 (Supplementary Fig. 1b). Antibodies against the other EMT-TFs SLUG (encoded by *SNAI2)* and SMUC (encoded by *SNAI3)* were not included in the RPPA.

Our previous microarray and NanoString analyses had additionally identified *SNAI1* induction by the SERM 4OHT, which exhibits partial agonist activity in human ILC cell

lines [31]. Assessment of *SNAI1* levels by qRT-PCR in our panel of estrogen-deprived ER+ ILC and IDC cell lines revealed induction of *SNAI1* by 4OHT only in two of the ILC cell lines, MDA-MB-134-VI and Sum44PE, and not in any of the IDC cells (Fig. 1a). Immunoblot analysis in these two cell lines confirmed that E2 and 4OHT lead to induction of SNAIL protein as well (Fig. 1c, Supplementary Fig. 2). Collectively, these data demonstrate that 4OHT induces the expression of the ER target SNAIL, a phenotype unique to a subset of human ILC cell lines.

ER is Recruited to the Promoter of SNAI1

SNAI1 is an established ER target gene in ER+ breast cancer cells [44, 45], but has not previously been reported to be induced by 4OHT. To assess if the induction of *SNAI1* by ER occurs directly, we first assessed ER binding at estrogen response elements (EREs) directly upstream of the *SNAI1* promoter. Data mined from the Ross-Innes ER ChIP database [46] revealed ER binding to an ERE, located approximately 1 kbp upstream of the *SNAI1* transcriptional start site, in multiple ER+ breast cancer cell lines, as well as in primary and metastatic lesions (Fig. 2a). We next performed ER ChIP in E2-deprived MDA-MB-134-VI cells after treatment with E2 or 4OHT for 8 hours, followed by qRT-PCR using primers flanking the ERE site. The specificity of the ChIP was confirmed by the observed ER binding to the promoter of its classical target *GREB1* but not to a non-functional ERE (*NFERE*) used as a negative control. Both E2 and 4OHT induced ER recruitment to the ERE upstream of the *SNAI1* promoter at this time point (Fig. 2b). We simultaneously performed immunoprecipitations of ER on our ChIP lysates to assess the efficiency of the pulldowns, and also confirmed the upregulation of *SNAI1* with mRNA analyses run concurrently with our ChIP experiment (Supplementary Fig. 3a, 3b). This experiment was additionally performed at two earlier time points, 45 minutes and 3 hours, though significant recruitment of ER was only observed at the 8 hour time point in response to 4OHT (Supplementary Fig. 3c, 3d). These data established the recruitment of ER to the *SNAI1* promoter in ILC cells, which is enhanced in the presence of E2 and 4OHT.

EMT-TF Programs are Upregulated in Some ILC Cell Lines

Although we did not observe significant E2-regulation of other EMT-related genes, it was possible that the baseline levels of EMT-TFs were higher in ILC vs. IDC cell lines. To directly investigate this, we measured mRNA expression of SNAIL, other EMT-TFs, and their downstream targets in a panel of ER+ ILC and IDC cell lines. All ILC cell lines utilized were first confirmed to have expression of ER and the ILC-hallmark loss of E-cadherin protein, with the exception of MDA-MB-330, which does express E-cadherin but has loss of adherens junctions due to a mutation in alpha catenin (Supplementary Fig. 4) [47]. Upregulation of *SNAI1*, as well as an additional EMT-TF, *TWIST1*, was consistently seen across several ILC cell lines as opposed to IDC cells (Fig. 3a; top panel). We additionally probed the mRNA expression of the EMT-TF downstream targets *CDH2* (N-cadherin), *FN1* (Fibronectin), and *VIM* (Vimentin), and observed similar patterns of upregulation in ILC cell lines relative to IDCs (Fig. 3a; bottom panel). Furthermore, we measured the endogenous protein expression of SNAIL and TWIST1 and observed higher levels in the ILC cell lines MDA-MB-134-VI and Sum44PE compared to other cell lines (Fig. 3b–c). As SNAIL and TWIST1 have previously been shown to have very short half-

lives (20–45 minutes) in cells, we additionally treated cells with the proteasome inhibitor MG132 and observed markedly stabilized levels for these proteins [48]. Taken together, these data implicate the existence of an EMT-like program in the majority of the commonly used ILC cell line models.

Transient SNAI1 Knockdown Leads to Increased Proliferation

We next set out to determine the functional consequences SNAIL inhibition in ILC cell lines. Our repeated attempts at generating cells with stable *SNAI1* knockdown were unsuccessful; however, we were able to decrease SNAIL levels using transient siRNA approaches. We initially knocked down *SNAI1* in MDA-MB-134-VI cells using siRNAs following E2-deprivation and assessed cell proliferation over 14 days. This transient *SNAI1* inhibition led to a surprising increase in E2-induced growth (Supplementary Fig. 5a) and a trend towards a mild decrease in 4OHT partial agonism (Supplementary Fig. 5b), although no statistically significant differences were observed between the EC50s for either treatment. We next transiently knocked down *SNAI1* in full serum in MDA-MB-134-VI cells, which exhibit the highest levels of endogenous SNAIL expression. We confirmed successful *SNAI1* knockdown, which was sustained over the 6-day experimental course (Fig. 4a). In agreement with the effect of *SNAI1* inhibition in E2-induced growth following E2 deprivation, *SNAI1* siRNA also resulted in increased proliferation of cells in full serum (Fig. 4b), a surprising result given the previously described role of SNAIL as a driver of cell proliferation in other contexts [49]. We also checked the effect of transient *SNAI1* knockdown on the expression of the downstream EMT-TF target genes and observed that only *FN1* was significantly decreased while there was no effect on *VIM* or *CDH2* (Fig. 4c).

SNAIL Overexpression Inhibits 2D and 3D Proliferation of ILC cells

To complement the loss-of-function studies described above, we generated stable, Doxycycline (Dox)-inducible SNAIL overexpressing models from ILC cell lines with low endogenous expression, specifically BCK4, MDA-MB-330, and Sum44PE cells. Treatment of these cell lines with Dox induced SNAIL protein expression and suppressed cell growth (Fig. 5a), corroborating the increased cell growth results from the loss-of-function studies in MDA-MB-134-VI cells. Given our observation of 4OHT-induced SNAIL expression, we asked whether ectopic overexpression of SNAIL was sufficient to elicit a partial agonist response to 4OHT treatment in BCK4, MDA-MB-330, and Sum44PE cells, and only observed a small but not significant effect in MDA-MB-330 cells (Supplementary Fig. 6). Instead, SNAIL overexpression generally repressed proliferation in the presence of 4OHT, consistent with its effects in full serum. Interestingly, a study by Vega et al has linked SNAIL overexpression to decreased proliferation, and cell cycle arrest [50]. We therefore assessed the cell cycle profiles of our inducible SNAIL overexpressing cells (Supplementary Fig. 7a). While cell cycle distribution of BCK4 control cells was not affected by treatment with Dox (Supplementary Fig. 7b), inducible overexpression of SNAIL led to arrest in the G_0/G_1 phase of the cell cycle, and decreased percentages of BCK4 cells in the S and G_2/M phases (Fig. 5b), with similar effects in MDA-MB-330 and Sum44PE cells (Supplementary Fig. 7c–d). In addition, we also assayed apoptosis and observed a marked reduction in the percentage of viable cells upon dox treatment only in BCK4 cells, concomitant with cleavage of PARP (Supplementary Fig. 7e–f).

We have recently reported a comprehensive phenotypic characterization of human ILC cell lines in 2D and 3D cultures [39]. To assess the effects of SNAIL in these biological phenotypes, we next assayed the effect of SNAIL overexpression on 3D growth and invasion ability plating the cells in 3D ECM gels: i) seeding on top of Matrigel ii) embedding within Matrigel or iii) embedding within Collagen I, conditions that mimic the stroma-rich growth of ILC cells *in vivo*. We then measured the formation of colonies with or without induction of SNAIL over a period of 24 days. While BCK4 and MDA-MB-330 did not form robust colonies in any environment, with or without SNAIL induction, colonies formed by Sum44PE cells were suppressed upon induction of SNAIL in all three environments (Fig. 5c). Finally, we asked if SNAIL regulated ILC mammosphere formation, an assay that has been used to assess stem cell-like properties of cancer cell lines [51]. As observed in Matrigel and collagen matrices, BCK4 and MDA-MB-330 were unable to form robust mammospheres, but instead formed loosely attached multi-cellular structures (Supplementary Fig. 8). In Sum44PE cells, induction of SNAIL led to significant reduction of mammosphere formation (Fig. 5d). Taken together, overexpression of SNAIL inhibited 2D growth and EMT-like phenotypes in the ILC cell line models, a somewhat surprising result based on the previously described roles of SNAIL in other biological systems [27–32, 48]. Nevertheless, the data from both our loss-of-function and overexpression studies complemented each other, suggesting a unique, context-dependent molecular role for SNAIL in ILC.

Discussion

Endocrine therapies have served as an arsenal of targeted treatments against ER+ breast cancers, but not without the rise of various resistance mechanisms. While the majority of ILCs respond very well to endocrine therapy, there is increasing evidence that tamoxifen treatment does not yield the desired outcome in a subset of patients [52]. The Cancer Genome Atlas (TCGA) ILC working group was among the first to publish a clear molecular distinction between ILC and IDC, including significant differences in PTEN, PI3K, FOXA1 and GATA3 mutations/activation between ILC and IDC [4]. However, limited studies have addressed potential differences in ER action, including estrogen and antiestrogen response [26, 41, 52–55].

Here, we identified SNAIL as a potential molecular target of 4OHT in tamoxifen-resistant ILC. Our data indicates that 4OHT can act as a partial agonist with respect to SNAIL induction in ILC cell lines. We found that this agonist behavior was limited to two of our ER + ILC cell lines, MDA-MB-134-VI and Sum44PE. Lack of response in MDA-MB-330 and BCK4 could indicate that these lines represent different histological and/or molecular subtypes within ILC, but further studies will need to delineate this in more detail. Our gene expression data is complemented by results from ChIP assays showing direct binding of ER to the promoter region of *SNAI1*, thereby providing additional support for the hypothesis that 4OHT can act as an agonist in ILC as opposed to an antagonist.

Our study was hampered by technical limitations in efficiently regulating SNAIL expression, potentially reflecting a very tight regulation of its levels in ILC cells. Nevertheless, results from our transient knockdown and inducible overexpression of SNAIL suggest that there is a

negative correlation between SNAIL levels and 2D and 3D growth. These data were surprising, since the majority of studies have described SNAIL as a positive regulator of growth and invasive properties, including in breast cancer [27–32, 48]. There is, however, prior precedence for SNAIL overexpression inhibiting cell cycle progression – Vega et al showed that SNAIL overexpression can cause cell cycle arrest and thereby protection from apoptosis [50]. It is reasonable to postulate that SNAIL overexpression in ILC cells might allow the cells to enter a quiescent state in which energy is conserved and cells are able to evade therapy for extended periods of time, indicative of tumor dormancy [56]. Future studies will be needed to further test this hypothesis, and to determine if these findings could be related to the observed late recurrences in patients with ER+ ILC [8, 15, 19–22]. Alternatively, SNAIL could be tightly regulated in a temporal context, something not addressed by these studies. Though SNAIL is induced by binding of ER to the *SNAI1* promoter circa 8 hours post 4OHT treatment and subsequent induction of expression and protein can be observed within a day of this induction, it is possible that this is then repressed at a later time point to allow for the overall 4OHT proliferation phenotype observed [26]. This temporal regulation of SNAIL will be pursued in future studies. Finally, it will also be critical to study potential contribution of other EMT genes, even if not directly regulated by SERMs, as especially TWIST1 that has been described to be highly expressed in ILC and its non-obligate precursor, Lobular Carcinoma *In Situ* (LCIS) [37].

In conclusion, we have shown that in some ILC models, 4OHT can act as an ER agonist with respect to regulation of SNAIL, a classical EMT-TF. SNAIL levels are tightly regulated in ILC cell lines, but inducible overexpression causes growth inhibition, associated with cell cycle arrest and apoptosis. These unexpected and hormone-independent quiescent phenotypes could contribute to tumor dormancy and therapeutic resistance, a hypothesis that need to be tested in future studies. Such studies are required to better understand the etiology of ILC, with the ultimate goal to personalize treatment for this patient population.

Supplementary Material

Refer to Web version on PubMed Central for supplementary material.

Acknowledgements

References

1. Howlader N, N.A., Krapcho M, Miller D, Bishop K, Kosary CL, et al. SEER Cancer Statistics Review, 1975–2014 2017 4 2017; Based on November 2016 SEER data submission].

2. Society AC Cancer Facts and Figures 2017 2017.

3. Barroso-Sousa R and Metzger-Filho O, Differences between invasive lobular and invasive ductal carcinoma of the breast: results and therapeutic implications. Ther Adv Med Oncol, 2016 8(4): p. 261–6. [PubMed: 27482285]

4. Ciriello G, et al., Comprehensive Molecular Portraits of Invasive Lobular Breast Cancer. Cell, 2015 163(2): p. 506–19. [PubMed: 26451490]

5. Christgen M, et al., Lobular breast cancer: Clinical, molecular and morphological characteristics. Pathol Res Pract, 2016 212(7): p. 583–97. [PubMed: 27233940]

6. Desmedt C, et al., Transcriptomic and genomic features of invasive lobular breast cancer. Semin Cancer Biol, 2017 44: p. 98–105. [PubMed: 28400203]

7. Malhotra GK, et al., Histological, molecular and functional subtypes of breast cancers. Cancer Biol Ther, 2010 10(10): p. 955–60. [PubMed: 21057215]

8. Arpino G, et al., Infiltrating lobular carcinoma of the breast: tumor characteristics and clinical outcome. Breast Cancer Res, 2004 6(3): p. R149–56. [PubMed: 15084238]

9. McCart Reed AE, et al., Invasive lobular carcinoma of the breast: morphology, biomarkers and 'omics. Breast Cancer Res, 2015 17(12): p. 12. [PubMed: 25849106]

10. Johnson K, Sarma D, and Hwang ES, Lobular breast cancer series: imaging. Breast Cancer Res, 2015 17(94): p. 94. [PubMed: 26163296]

11. Sobinsky JD, et al., Unusual metastatic patterns of invasive lobular carcinoma of the breast. Case Rep Oncol Med, 2013 2013: p. 986517. [PubMed: 24324904]

12. Shakoor MT, et al., Unique presentations of invasive lobular breast cancer: a case series. Int J Biomed Sci, 2014 10(4): p. 287–93. [PubMed: 25598762]

13. Mathew A, et al., Distinct Pattern of Metastases in Patients with Invasive Lobular Carcinoma of the Breast. Geburtshilfe Frauenheilkd, 2017 77(6): p. 660–666. [PubMed: 28757653]

14. Lumachi F, et al., Endocrine therapy of breast cancer. Curr Med Chem, 2011 18(4): p. 513–22. [PubMed: 21143113]

15. Chen Z, et al., Invasive lobular carcinoma of the breast: A special histological type compared with invasive ductal carcinoma. PLoS One, 2017 12(9): p. e0182397. [PubMed: 28863134]

16. Jordan VC, Tamoxifen as the first targeted long-term adjuvant therapy for breast cancer. Endocr Relat Cancer, 2014 21(3): p. R235–46. [PubMed: 24659478]

17. Milani A, et al., Overcoming endocrine resistance in metastatic breast cancer: Current evidence and future directions. World J Clin Oncol, 2014 5(5): p. 990–1001. [PubMed: 25493235]

18. Smith BN and Bhowmick NA, Role of EMT in Metastasis and Therapy Resistance. J Clin Med, 2016 5(2).

19. Pestalozzi BC, et al., Distinct clinical and prognostic features of infiltrating lobular carcinoma of the breast: combined results of 15 International Breast Cancer Study Group clinical trials. J Clin Oncol, 2008 26(18): p. 3006–14. [PubMed: 18458044]

20. Narbe U, et al., Invasive lobular carcinoma of the breast: long-term prognostic value of Ki67 and histological grade, alone and in combination with estrogen receptor. Springerplus, 2014 3: p. 70. [PubMed: 24567879]

21. Engstrøm MJ, et al., Invasive lobular breast cancer: the prognostic impact of histopathological grade, E-cadherin and molecular subtypes. Histopathology, 2015 66: p. 409–19. [PubMed: 25283075]

22. Adachi Y, et al., Comparison of clinical outcomes between luminal invasive ductal carcinoma and luminal invasive lobular carcinoma. BMC Cancer, 2016 16: p. 248. [PubMed: 27015895]

23. Araki K and Miyoshi Y, Mechanism of resistance to endocrine therapy in breast cancer: the important role of PI3K/Akt/mTOR in estrogen receptor-positive, HER2-negative breast cancer. Breast cancer (Tokyo, Japan), 2017 25: p. 392–401.

24. Chang M, Tamoxifen resistance in breast cancer. Biomol Ther (Seoul), 2012 20(3): p. 256–67. [PubMed: 24130921]

25. Ali S, et al., Molecular mechanisms and mode of tamoxifen resistance in breast cancer. Bioinformation, 2016 12(3): p. 135–139. [PubMed: 28149048]

26. Sikora MJ, et al., Invasive lobular carcinoma cell lines are characterized by unique estrogen-mediated gene expression patterns and altered tamoxifen response. Cancer Res, 2014 74(5): p. 1463–74. [PubMed: 24425047]

27. de Herreros AG, et al., Snail family regulation and epithelial mesenchymal transitions in breast cancer progression. J Mammary Gland Biol Neoplasia, 2010 15(2): p. 135–47. [PubMed: 20455012]

28. Martin TA, et al., Expression of the transcription factors snail, slug, and twist and their clinical significance in human breast cancer. Ann Surg Oncol, 2005 12(6): p. 488–96. [PubMed: 15864483]

29. Peinado H, Olmeda D, and Cano A, Snail, Zeb and bHLH factors in tumour progression: an alliance against the epithelial phenotype? Nat Rev Cancer, 2007 7(6): p. 415–28. [PubMed: 17508028]

30. Moody SE, et al., The transcriptional repressor Snail promotes mammary tumor recurrence. Cancer Cell, 2005 8(3): p. 197–209. [PubMed: 16169465]

31. Elloul S, et al., Snail, Slug, and Smad-interacting protein 1 as novel parameters of disease aggressiveness in metastatic ovarian and breast carcinoma. Cancer, 2005 103(8): p. 1631–43. [PubMed: 15742334]

32. Dubois-Marshall S, et al., Two possible mechanisms of epithelial to mesenchymal transition in invasive ductal breast cancer. Clin Exp Metastasis, 2011 28(8): p. 811–8. [PubMed: 21789718]

33. Chen WJ, et al., Multidrug resistance in breast cancer cells during epithelial-mesenchymal transition is modulated by breast cancer resistant protein. Chin J Cancer, 2010 29(2): p. 151–7. [PubMed: 20109342]

34. Kajita M, McClinic KN, and Wade PA, Aberrant expression of the transcription factors snail and slug alters the response to genotoxic stress. Mol Cell Biol, 2004 24(17): p. 7559–66. [PubMed: 15314165]

35. Proia TA, et al., Genetic predisposition directs breast cancer phenotype by dictating progenitor cell fate. Cell Stem Cell, 2011 8(2): p. 149–63. [PubMed: 21295272]

36. McCart Reed AE, et al., An epithelial to mesenchymal transition programme does not usually drive the phenotype of invasive lobular carcinomas. J Pathol, 2016 238(4): p. 489–94. [PubMed: 26510554]

37. Morrogh M, et al., Cadherin-catenin complex dissociation in lobular neoplasia of the breast. Breast Cancer Res Treat, 2012 132(2): p. 641–52. [PubMed: 22080244]

38. Jambal P, et al., Estrogen switches pure mucinous breast cancer to invasive lobular carcinoma with mucinous features. Breast Cancer Res Treat, 2013 137(2): p. 431–48. [PubMed: 23247610]

39. Tasdemir N, et al., Comprehensive Phenotypic Characterization of Human Invasive Lobular Carcinoma Cell Lines in 2D and 3D Cultures. Cancer Res, 2018 78(21): p. 6209–6222. [PubMed: 30228172]

40. Meerbrey KL, et al., The pINDUCER lentiviral toolkit for inducible RNA interference in vitro and in vivo. Proc Natl Acad Sci U S A, 2011 108(9): p. 3665–70. [PubMed: 21307310]

41. Sikora MJ, et al., WNT4 mediates estrogen receptor signaling and endocrine resistance in invasive lobular carcinoma cell lines. Breast Cancer Res, 2016 18(1): p. 92. [PubMed: 27650553]

42. Shaw FL, et al., A detailed mammosphere assay protocol for the quantification of breast stem cell activity. J Mammary Gland Biol Neoplasia, 2012 17(2): p. 111–7. [PubMed: 22665270]

43. Harrell JC, Shroka TM, and Jacobsen BM, Estrogen induces c-Kit and an aggressive phenotype in a model of invasive lobular breast cancer. Oncogenesis, 2017 6(11): p. 396. [PubMed: 29176653]

44. Scherbakov AM, et al., The relationships between snail1 and estrogen receptor signaling in breast cancer cells. J Cell Biochem, 2012 113(6): p. 2147–55. [PubMed: 22307688]

45. Wang M, et al., AIB1 cooperates with ERalpha to promote epithelial mesenchymal transition in breast cancer through SNAI1 activation. PLoS One, 2013 8(6): p. e65556. [PubMed: 23762395]

46. Ross-Innes CS, et al., Differential oestrogen receptor binding is associated with clinical outcome in breast cancer. Nature, 2012 481(7381): p. 389–93. [PubMed: 22217937]

47. Christgen M and Derksen P, Lobular breast cancer: molecular basis, mouse and cellular models. Breast Cancer Res, 2015 17: p. 16. [PubMed: 25757734]

48. Zhou BP, et al., Dual regulation of Snail by GSK-3beta-mediated phosphorylation in control of epithelial-mesenchymal transition. Nat Cell Biol, 2004 6(10): p. 931–40. [PubMed: 15448698]

49. Lundgren K, Nordenskjold B, and Landberg G, Hypoxia, Snail and incomplete epithelial-mesenchymal transition in breast cancer. Br J Cancer, 2009 101(10): p. 1769–81. [PubMed: 19844232]

50. Vega S, et al., Snail blocks the cell cycle and confers resistance to cell death. Genes Dev, 2004 18(10): p. 1131–43. [PubMed: 15155580]

51. Mani SA, et al., The epithelial-mesenchymal transition generates cells with properties of stem cells. Cell, 2008 133(4): p. 704–15. [PubMed: 18485877]

52. Metzger Filho O, et al., Relative Effectiveness of Letrozole Compared With Tamoxifen for Patients With Lobular Carcinoma in the BIG 1–98 Trial. J Clin Oncol, 2015 33(25): p. 2772–9. [PubMed: 26215945]

53. Riggins RB, et al., ERRgamma mediates tamoxifen resistance in novel models of invasive lobular breast cancer. Cancer Res, 2008 68(21): p. 8908–17. [PubMed: 18974135]

54. Stires H, et al., Integrated molecular analysis of Tamoxifen-resistant invasive lobular breast cancer cells identifies MAPK and GRM/mGluR signaling as therapeutic vulnerabilities. Mol Cell Endocrinol, 2018 471: p. 105–117. [PubMed: 28935545]

55. van Agthoven T, et al., Breast Cancer Anti-Estrogen Resistance 4 (BCAR4) Drives Proliferation of IPH-926 lobular Carcinoma Cells. PLoS One, 2015 10(8): p. e0136845. [PubMed: 26317614]

56. Sosa MS, Bragado P, and Aguirre-Ghiso JA, Mechanisms of disseminated cancer cell dormancy: an awakening field. Nat Rev Cancer, 2014 14(9): p. 611–22. [PubMed: 25118602]
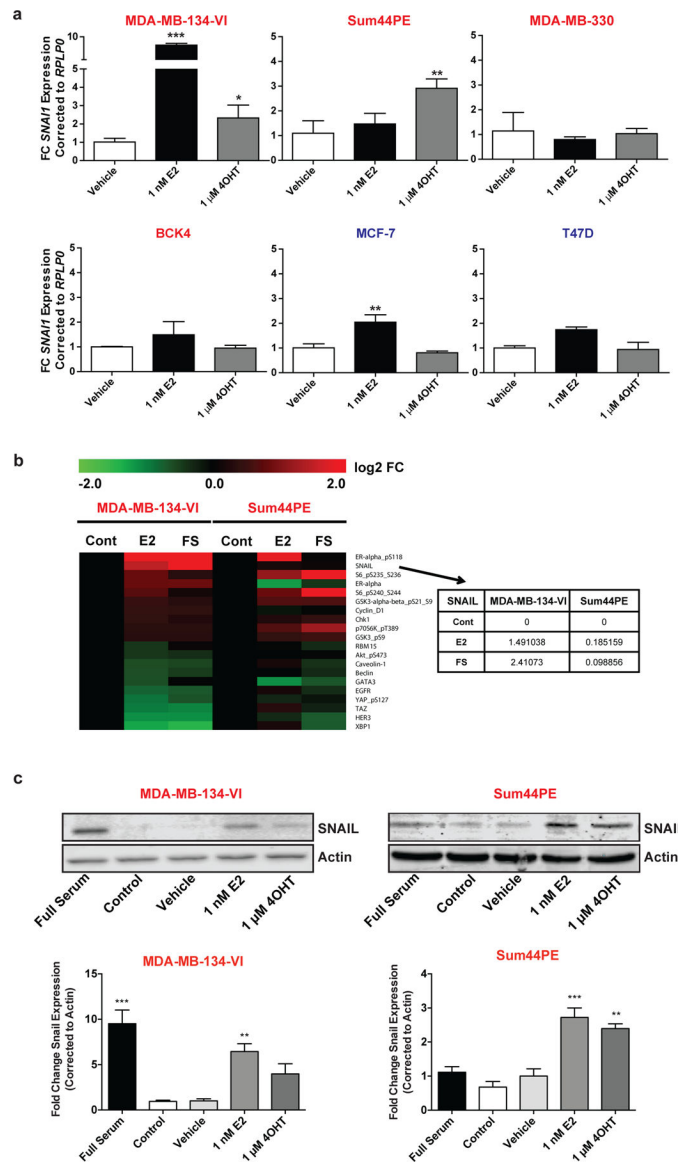
Fig. 1.
4OHT Acts as an Agonist in ER+ ILC Cells. **a** *SNAI1* qRT-PCR assessment of ILC (red) and IDC (blue) cells was performed at 24 hours post deprivation/treatments (Vehicle 0.1% DMSO). Quantifications are a representative single experiment ± STDEV of technical triplicates, with similar results in two additional independently performed experiments. Asterisks depict significance compared to Vehicle from One Way ANOVA followed by Tukey's post-test. **b** RPPA analysis of MDA-MB-134-VI and Sum44PE cells in Full Serum (FS) or deprived of exogenous estrogens (Cont) followed by treatment with 1 nM E2 for 24 hours. Top ten E2-upregulated and downregulated proteins in MDA-MB-134-VI cells are displayed. Log2 fold change (FC) for SNAIL is depicted in the table. (C) SNAIL immunoblots were performed in MDA-MB-134-VI and Sum44PE cells at 24 hours post deprivation/treatments. Representative images are displayed (top) along with quantification of band intensities (bottom). Graphs represent mean +/− standard error relative to Vehicle
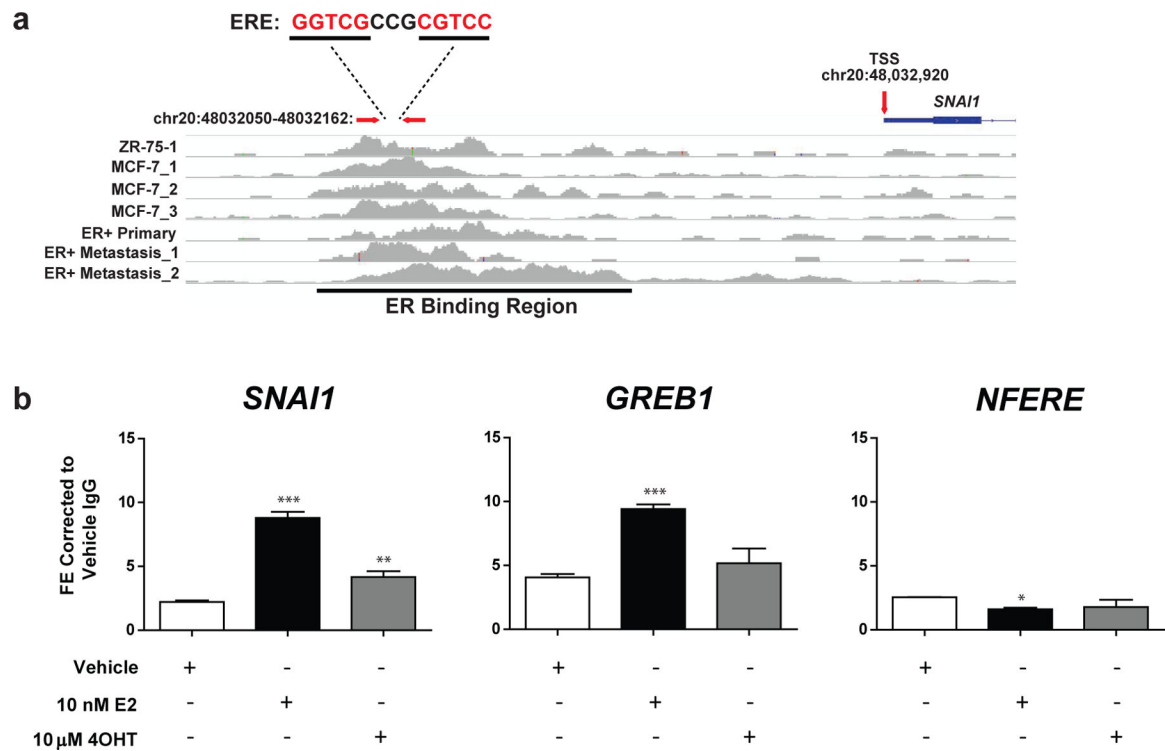
from independent experiments (n=3). Asterisks depict significance compared to Vehicle from One Way ANOVA followed by Dunnett's post-test. (*p<0.05, **p<0.005, ***p<0.0005)

Fig. 2.
ER is Recruited to the Promoter of *SNAI1*. **a** Conserved EREs upstream of the *SNAI1* transcriptional start site (TSS) from *in silico* analyses of publicly available ER ChIP data were identified. Build hg18 was used. The general ER binding region is underlined. Arrows indicate the position of designed ChIP qRT-PCR primers and the TSS, and an excerpt shows the ERE in the ChIP qRT-PCR primer region with base pairs from the ER motif shown in red font and spacer base pairs in black font. The primer region is 1 kbp upstream of the TSS. **b** ER ChIP was performed in MDA-MB-134-VI cells after a period of three days of estrogen deprivation and treatment with vehicle (0.1% DMSO), E2, or 4OHT for 8 hours. ChIP qRT-PCR was performed and displayed as mean ± STDEV of technical triplicates relative to vehicle IgG control for region of interest *SNAI1*, positive E2 control *GREB1*, and negative control *NFERE*. Statistics were performed using One Way ANOVA followed by Tukey's post-test (*p<0.05, **p<0.005, ***p<0.0005) with comparison relative to vehicle control displayed with asterisks. Data are representative of two independently performed experiments
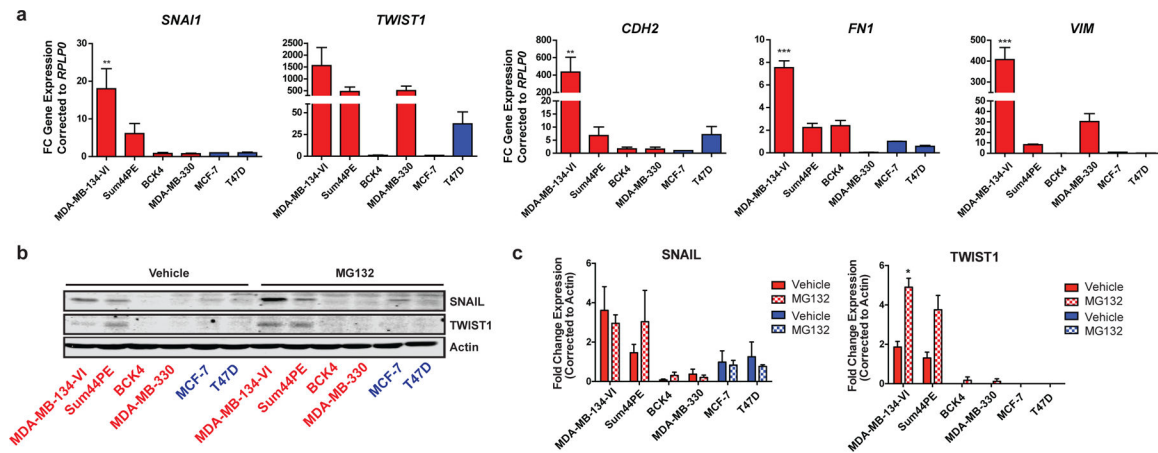
Fig. 3.
EMT-TF Related Genes are Upregulated in ILC. **a** mRNA and **b** protein expression of two
EMT-TFs and downstream EMT targets in ILC (red) and IDC (blue) ER+ cells. Combined
qRT-PCR data from three independent experiments are shown relative to MCF-7 as means ±
SEM. One Way ANOVA followed by Tukey's post-test are displayed with asterisks
comparing cells to MCF-7 expression of a gene of interest. Immunoblot is representative of
a set of three independently performed experiments ± 5 μM MG132 treatment for two hours.
c Quantification of band intensities from **b**. Graphs represent mean +/− standard error
relative to Vehicle from independent experiments (n=3). Asterisks depict significance from
t-tests followed by correction for multiple comparisons using the Holm-Sidak method.
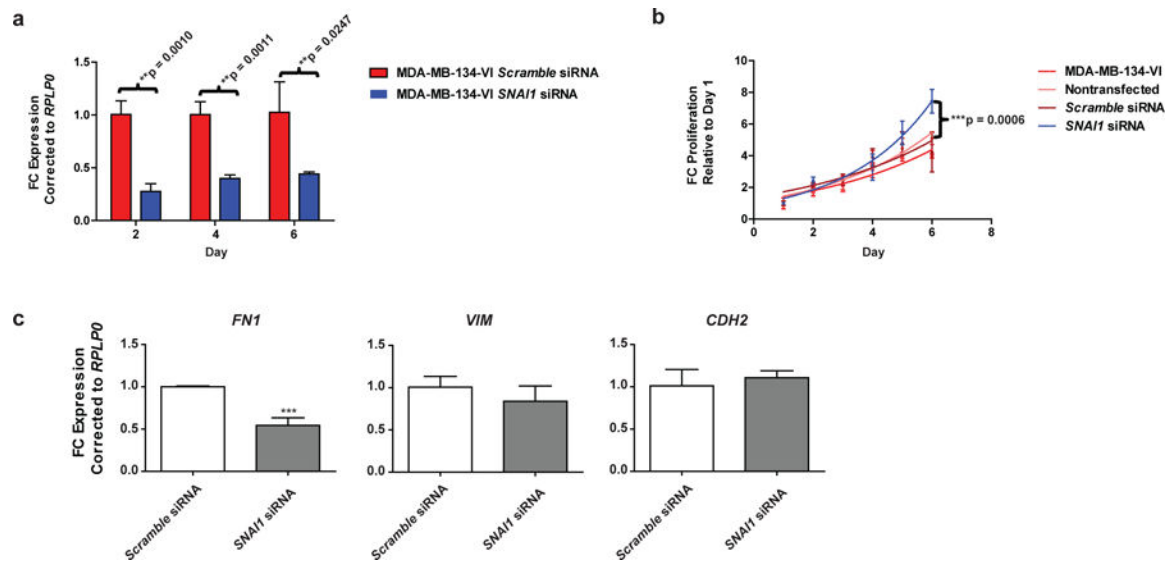(*p<0.05, **p<0.005, ***p<0.0005)

Fig. 4.

Transient *SNAI1* Knockdown Leads to Decreases in Few EMT-TF Targets and Increases Proliferation. Transient knockdown of SNAI1 was performed in 2D plates with *Scramble* or *SNAI1* siRNA. **a** qRT-PCR confirmation of transient knockdown of *SNAI1* throughout experiment was completed at days two, four, and six with Student's t-test evaluations shown. Data represent three independently repeated experiments. **b** Representative 2D proliferation data corrected to background media fluorescence and shown relative to day one values. Non-linear regression exponential growth curves were fitted and a comparison of growth rates was performed; significance between *Scramble* and *SNAI1* siRNA groups is displayed. **c** Representative qRT-PCR data of probed downstream EMT-TF targets are displayed as means relative to *Scramble* ± STDEV of technical triplicates with One Way ANOVA followed by Tukey's post-test (*p<0.05, **p<0.005, ***p<0.0005) displayed by asterisks. Data represent two independently repeated experiments. MDA-MB-134-VI: no transfection reagent or siRNA. Nontransfected: transfection reagent only; no siRNA
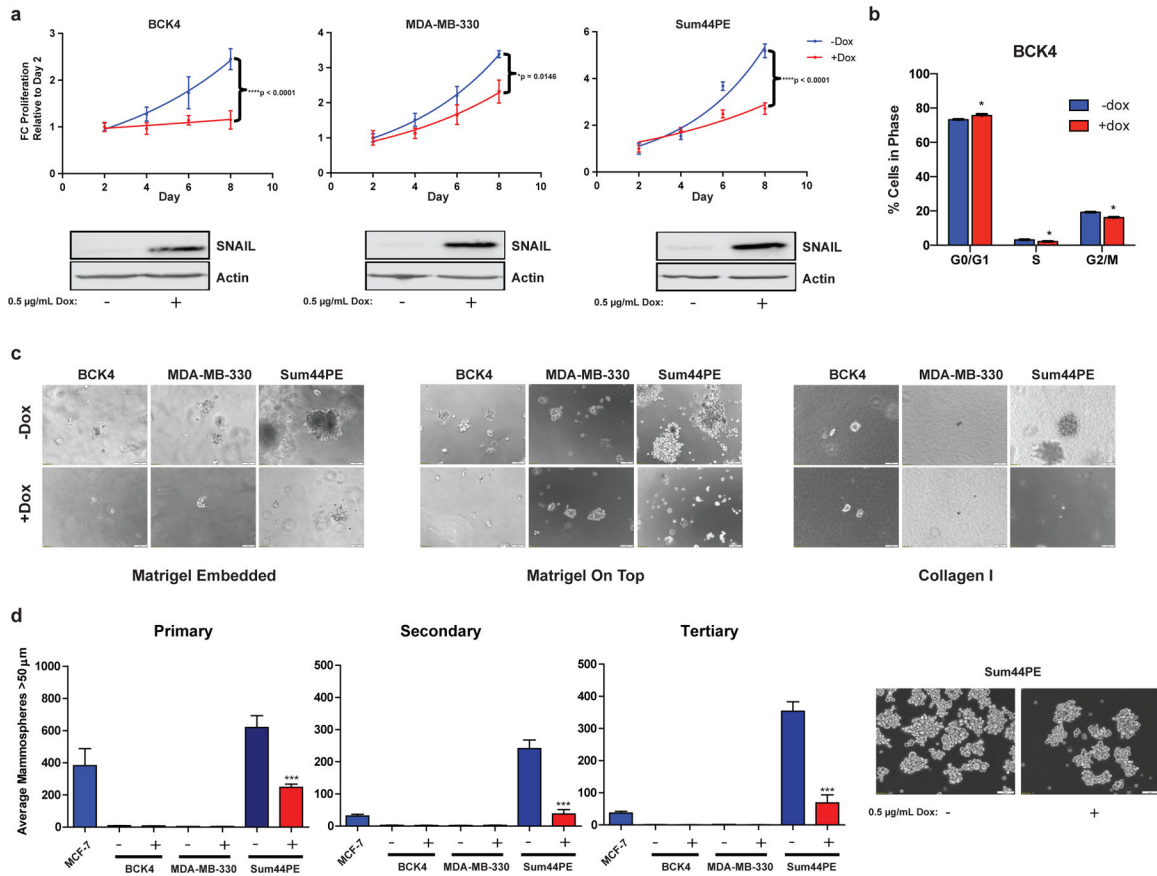
Fig. 5.

SNAIL Overexpression Causes Decreased Proliferative, Invasive, and Stem-Like Phenotypes. Inducible SNAIL overexpression ILC BCK4, MDA-MB-330, and Sum44PE cells were treated to ± Dox in **a** 2D environments followed by **b** evaluation of cell cycle profiles for BCK4 cells at day 4. Data in **b** are representative of two independently performed experiments with three technical replicates per experiment ± STDEV and asterisks depict significance from t-tests followed by correction for multiple comparisons using the Holm-Sidak method. In addition, cells were probed for phenotypic changes in **c** 3D environments, or **d** in a mammosphere assay. Scale bars represent 50 μm. Proliferation curves and protein were assessed as previously. Data in **a** are a representative experiment of three independently performed experiments with six technical replicates per time point ± STDEV, displayed relative to day 2. Data in **d** are three independently performed experiment means ± SEM, each performed with technical triplicates. One Way ANOVA followed by Tukey's post-test (*p<0.05, ***p<0.0005; ****p<0.0001), are displayed with asterisks comparing ± Dox treatment. Images from **c** and **d** represent phase images at day 24 or day 17, respectively, 20X magnification